MCB
Journals.ASM.org

Cellular Adaptation to Anthrax Lethal Toxin-Induced Mitochondrial Cholesterol Enrichment, Hyperpolarization, and Reactive Oxygen Species Generation through Downregulating MLN64 in Macrophages

Soon-Duck Ha, Sangwook Park, Chae Young Han, Marilyn L. Nguyen, and Sung Ouk Kim

Department of Microbiology and Immunology and Centre for Human Immunology, Siebens-Drake Research Institute, University of Western Ontario, London, Ontario, Canada

Cellular adaptation to different stresses related to survival and function has been demonstrated in several cell types. Anthrax lethal toxin (LeTx) induces rapid cell death, termed "pyroptosis," by activating NLRP1b/caspase-1 in murine macrophages. We and others (S. D. Ha et al., J. Biol. Chem. 282:26275-26283, 2007; I. I. Salles et al., Proc. Natl. Acad. Sci. U. S. A. 100:12426–12431, 2003) have shown that RAW264.7 cells preexposed to sublethal doses of LeTx become resistant to subsequent high cytolytic doses of LeTx, termed toxin-induced resistance (TIR). To date, the cellular mechanisms of pyroptosis and TIR are largely unknown. We found that LeTx caused NLRP1b/caspase-1-dependent mitochondrial dysfunction, including hyperpolarization and generation of reactive oxygen species, which was distinct from that induced by stimuli such as NLRP3-activating ATP. In TIR cells, these mitochondrial events were not detected, although caspase-1 was activated, in response to LeTx. We identified that downregulation of the late endosomal cholesterol-transferring protein MLN64 in TIR cells was involved in TIR. The downregulation of MLN64 in TIR cells was at least in part due to DNA methyltransferase 1-mediated DNA methylation. In wild-type RAW264.7 cells and primary bone marrow-derived macrophages, LeTx caused NLRP1b/caspase-1-dependent mitochondrial translocation of MLN64, resulting in cholesterol enrichment, membrane hyperpolarization, reactive oxygen species (ROS) generation, and depletion of free glutathione (GSH). This study demonstrates for the first time that MLN64 plays a key role in LeTx/caspase-1-induced mitochondrial dysfunction.

Anthrax lethal toxin (LeTx), which comprises the intracellular transporter protective antigen and the metalloprotease lethal factor (LF), is a key virulence factor of *Bacillus anthracis*, the causative agent of anthrax. After entry into the cell, LF causes the release of inflammatory cytokines, such as interleukin 1β (IL-1β) and IL-18, and rapid cell death, termed "pyroptosis" in murine macrophages, where caspase-1 plays an integral role in both cleaving pro-IL-1β into biologically active IL-1β and executing cell death (61). LeTx-induced pyroptosis is known to be mediated by the formation of inflammasomes composed of the NOD-like receptor pyrin domain-containing protein 1b (NLRP1b) and caspase-1 (11). However, the downstream signaling events of caspase-1 involved in pyroptosis are still elusive. LF also directly cleaves and inactivates mitogen-activated protein kinase kinases (MAPKKs) 1 to 7, except MAPKK 5, resulting in an almost complete inactivation of extracellular signal-regulated kinases (ERKs), p38 mitogen-activated protein kinases (MAPKs), and c-Jun N-terminal kinases. However, it is not clear if inactivation of these signaling molecules is sufficient for or involved in inducing pyroptosis. Several other cellular events were shown to be associated with LeTx-induced pyroptosis, including early mitochondrial dysfunction (3, 28), lysosomal permeabilization (7), Ca^{2+} influx (8, 54), and generation of reactive oxygen species (ROS) (30). However, it still remains to be explored how these events are related to caspase-1 activation or pyroptosis.

Macrophages are forefront innate immune cells facing various microbial challenges and often adapt to different stresses to maintain vigilance or counterbalance overwhelming inflammatory responses. For example, macrophages gain tolerance to an endotoxin such as lipopolysaccharides after preexposure to the endotoxin at a low dose (37, 68). Similarly, we and others have shown that macrophages preexposed to sublethal doses of LeTx are refractory to subsequent high cytolytic doses of LeTx (19, 28, 50), termed toxin-induced resistance (TIR). A small portion of TIR cells (2 to 4%) retain TIR characteristics for up to 5 to 6 weeks (28). These cells were shown to be normal in cleaving MAPKKs, suggesting that the adaptation to LeTx occurs at steps after LF is released into the cytoplasm (28). One study suggested that adaptive ERK activation by a MAPKK-independent process or a general decrease in proteasome activity could be involved in TIR (50). Although inactivation of ERK has not yet been demonstrated to be involved in pyroptosis, proteasome activity was shown to be involved in LeTx-induced pyroptosis (57, 64). We previously showed that TIR cells also downregulated mitochondrial cell death proteins such as Bcl2/adenovirus E1B-interacting protein 3 (BNIP3) and BNIP3L, suggesting that resistance to LeTx-induced mitochondrial dysfunction is also involved in TIR. However, how LF or caspase-1 induces mitochondrial dysfunction and how TIR cells become resistant to such effects are still unknown.

In addition to NLRP1b, caspase-1-dependent pyroptosis can be induced by other intracellular innate immune receptors, including NLRP3 (which senses various stimuli such as microbial

Received 16 April 2012 **Returned for modification** 28 May 2012
Accepted 24 September 2012
Published ahead of print 1 October 2012
Address correspondence to Sung Ouk Kim, sung.kim@schulich.uwo.ca.
Supplemental material for this article may be found at http://mcb.asm.org/.

doi:10.1128/MCB.00494-12

pore-forming toxins, crystalline uric acid or uric acid crystals, and extracellular ATP), NLRC4 (which is also known as IPAF and which senses the presence of flagellin), and AIM2 (which recognizes viral or double-stranded DNAs) (23). Interestingly, activation of these receptors and NLRP1b commonly involves cellular events such as K^+ efflux and reactive oxygen species (ROS) generation (26). However, these cellular events alone are not sufficient to activate the receptors, and they have been suggested to function as a safeguard for preventing inappropriate activation of pyroptosis. In other words, these receptors may employ unique sets of cellular events for their activation. Although activation of caspase-1 is an integral part of pyroptosis induced by these receptors, cell death processes and characteristics could also be different between these receptors. This study shows that LeTx/NLRP1b, unlike ATP/NLRP3, caused caspase-1-dependent mitochondrial events, including cholesterol enrichment, hyperpolarization, glutathione (GSH) depletion, ROS generation, and condensation. These mitochondrial events were mediated through the cholesterol-transferring protein MLN64 (metastatic lymph node 64), which was translocated from late endosomes to mitochondria. TIR cells were deficient in MLN64 and were resistant to these mitochondrial events and subsequent pyroptosis.

MATERIALS AND METHODS

Cells and cell culture. RAW264.7 cells were grown in Dulbecco's modified Eagle medium (DMEM) containing 8% heat-inactivated fetal bovine serum (Sigma-Aldrich), 10 mM MEM nonessential amino acids solution, 100 U/ml penicillin G sodium, 100 μg/ml streptomycin sulfate, and 1 mM sodium pyruvate. Cells were grown at 37°C in a humidified atmosphere with 5% CO_2. Primary bone marrow-derived macrophages (BMDMs) were obtained from 129/S1/Svlmj and DBA/2J mice as previously described (62). Bone marrow-derived immortalized macrophages (BMDIM) from C57BL/6J mice were generated as described previously (1, 62). Briefly, bone marrow cells were transfected with the J2 murine retrovirus, which carries the v-*raf* and v-*myc* oncogenes, and cultured for 7 days in macrophage-driving medium containing macrophage colony-stimulating factor (62). Cells were then cultured with normal medium (RPMI 1640 medium containing 10% heat-inactivated fetal bovine serum, 10 mM MEM nonessential amino acids solution, 100 U/ml penicillin G sodium, 100 μg/ml streptomycin sulfate, and 1 mM sodium pyruvate). TIR cells were generated as previously reported (28). Briefly, RAW264.7 cells were exposed to LeTx (500 ng/ml LF and 1 μg/ml PA) for 5 h, and surviving cells were plated in a fresh culture dish. Individual clones were picked 10 to 14 days after LeTx treatment and plated on a 96-well plate. Each clone was tested for LeTx sensitivity, and LeTx-resistant (TIR) clones were pooled and propagated.

Reagents. Lethal factor (LF) and protective antigen (PA) were prepared as previously described (28). ATP (adenosine 5′-triphosphate, disodium salt), nigericin, caspase-1 inhibitor 1, and 3-3′-dihexyloxacarbocyanine iodide ($DiOC_6$) were purchased from Calbiochem (EMD Biosciences, La Jolla, CA). Mito-Tempo was obtained from Enzo Life Sciences. Ammonium pyrrolidine dithiocarbamate (APDC), antimycin A, apocynin, azacytidine, filipin, diphenyleneiodonium chloride (DPI), methyl-β-cyclodextrin, rotenone, propidium iodide (PI), and tetramethylrhodamine methyl ester perchlorate (TMRM) were purchased from Sigma-Aldrich. The antibody raised against the NH_2 terminus of MEK1 was obtained from QED Bioscience Inc., and antibodies against the COOH terminus of MLN64, caspase-1, and SOD2 were purchased from Santa Cruz Biotechnology. Antibodies against p38 MAPK and estrogen receptor (ER) proteins (CHOP and IRE1α) were obtained from Cell Signaling Technologies, and β-actin was obtained from Rockland Inc. (Gilbertsville, PA). CM-H_2DCFDA (5 [and 6]-chloromethyl-2′,7′-dichlorodihydrofluorescein, acetyl ester, C6827), and Mitosox red (M36008) were obtained from Life Technologies (Invitrogen, Molecular Probes).

Cytotoxicity assay. A microtiter tetrazolium (MTT) assay or propidium iodide (PI) staining was used to assess cytotoxicity. For the MTT assay, RAW264.7 macrophages were cultured in the presence or absence of LeTx, ATP, or nigericin in 96-well plates, and MTT was then added at a final concentration of 0.5 mg/ml. After an additional 2 h of incubation at 37°C, culture media were carefully aspirated and 100 μl of dimethyl sulfoxide (DMSO) was added to dissolve formed crystals. Optical densities of the wells were analyzed using an automatic enzyme-linked immunosorbent assay (ELISA) plate reader (Bio-Rad) at a wavelength of 590 nm. The percent cell death was estimated by comparing the optical density of wells containing treated cells with the optical density of those containing nontreated cells, which was taken as representing no cell death. For propidium iodide (PI) staining, cells were cultured in the presence or absence of LeTx in 12- or 6-well plates and were harvested at the time indicated in the figures or figure legends. After washing twice, cells were resuspended in phosphate-buffered saline (PBS) containing 2 μg/ml PI at a density of 1 million cells/ml and analyzed by flow cytometry using a FACSCalibur cytometer (Becton-Dickinson Biosciences). The data were analyzed using CellQuest Pro software (Becton-Dickinson Biosciences).

Total cell lysate preparation and Western immunoblot analysis. Total cell lysate extraction and Western blot analysis were performed as previously described (29). For caspase-1 cleavage measurement, Western blots were performed on extracts prepared from cells and culture supernatants by adding lysis buffer (20 mM MOPS, 2 mM EGTA, 5 mM EDTA, 1 mM Na_3VO_4, 40 mM β-glycerophosphate, 30 mM sodium fluoride, and 20 mM sodium pyrophosphate [pH 7.2]) containing 1% Triton X-100 to cell cultures.

Active caspase-1 detection. Active caspase-1 was measured with a FLICA (fluorochrome inhibitor of caspase) system using a FAM-YVAD-FMK kit (Immunochemistry Technologies, LLC). Cells were labeled with FLICA solution according to the manufacturer's protocol. Cells were then fixed and further stained with 10 μg/ml Hoechst 33258 (Sigma-Aldrich) in PBS for 3 min to visualize nuclei. Cells were then observed using an Olympus fluorescence microscope at a magnification of 600×, and images were acquired using QCapture Pro (Media Cybernetics, Inc., and QImaging, Inc.).

Mitochondrial membrane polarization measurements. 3-3′-Dihexyloxacarbocyanine iodide ($DiOC_6$; Calbiochem) and TMRM (tetramethylrhodamine methyl ester perchlorate) were used to measure mitochondrial membrane polarization. Cells were treated with LeTx with or without inhibitors and then washed twice with prewarmed fresh medium and incubated with fresh medium containing $DiOC_6$ (2 μg/ml) at 37°C for 10 min. For TMRM staining, cells were incubated with TMRM (250 nM) for 30 min at 37°C. After two washes with fresh medium, cells were then harvested and analyzed using FACSCalibur (Becton-Dickinson Biosciences). The data were analyzed using CellQuest software (Becton-Dickinson Biosciences).

MitoTracker staining. A MitoTracker red CM-H_2X ROS (Invitrogen, Molecular Probes) probe was used for mitochondrial staining. Cells were stained and fixed by manufacturer's protocol, and fixed cells were observed by confocal microscopy (LSM510; Zeiss). Images were acquired using ZEN software.

ROS measurements. Macrophages were treated with LeTx and 5 μM CM-H_2DCFDA [5 (and 6)-chloromethyl-2′,7′-dichlorodihydrofluorescein, acetyl ester (Molecular Probes, Invitrogen)] for 30 min at 37°C to measure total cellular ROS generation. Similarly, mitochondrial ROS generation was assessed by staining cells with Mitosox red (2.5 μM; Invitrogen, Molecular Probes) for 15 min.

pDsRed-MLN64, pEGFP-MLN64, and pEGFP-GSTA4 constructs and transfection. For expression of red fluorescent protein (RFP)- or enhanced green fluorescent protein (eGFP)-tagged mouse MLN64, mouse MLN64 cDNAs were prepared from total RNA and amplified by PCR using gene (accession number NM021547)-specific primers (for-

ward, 5′-TAATGAATTCTAGCAAGCGACCTGGTGATCTG-3′; reverse, 5′-TAATGGATCCTCAAGCTCGGGCCCCCAGCT-3′) and cloned into pEGFP-C1 or pDsRed-monomer–C1 vector using EcoRI and BamHI restriction enzymes. The N-terminal eGFP-tagged GSTA4 plasmid (pEGFP-GSTA4) was constructed using mouse GSTA4 cDNA (accession number NM010357) amplified by PCR primers 5′-TAATGAATT CTGCAGCCAAACCTAAGCTCTACT-3′ (forward) and 5′-TAATGGA TCCCTAGAACTTCAGGACAGTCCTG-3′ (reverse). The amplified product was cloned into pEGFP-C1 vector using EcoRI and BamHI restriction enzymes. Lipofectamine 2000 (Invitrogen) was used for plasmid transfections into RAW 264.7 cells or TIR cells.

Small interfering RNA (siRNA). Pooled siRNAs directed against mouse MLN64 (NM 021547) were purchased from Thermo Scientific (On-Target-plus SMARTpool reagent; L-048833-01-0005). The mouse BNIP3L (NM 009761) siRNAs were purchased from Dharmacon (On-Target duplex; D-058953-01-0005; Thermo Scientific). Mouse caspase-1-specific siRNAs were obtained from Ambion (catalog no. 4390771) through Invitrogen, and mouse DNMT1 siRNAs were from Qiagen (catalog no. S100189910). siRNAs were transfected using Lipofectamine RNAi MAX (Invitrogen), following the manufacturer's instructions. Levels of mRNA expressions were confirmed by quantitative real-time PCR or Western blotting. Primers used for MLN64 were 5′-CAGGCAGTCAC CGTCTTGTT-3′ (5′ primer) and 5′-TGCGGTGGTGGATCAGATCT-3′ (3′ primer), and those for DNMT1 were 5′-AAGAATGGTGTTGTCTAC CGAC-3′ (5′ primer) and 5′-CATCCAGGTTGCTCCCTTG-3′ (3′ primer).

PCR array and quantitative real-time PCR. The mouse mitochondrial RT^2 Profiler PCR array system (mouse mitochondria, PAMM-087; SABiosciences, Qiagen) was used for expression profiling of mitochondrion-focused genes in RAW264.7 and TIR cells. Total RNAs were isolated using TRIzol reagent (Life Technologies) and further purified with a Qiagen RNeasy minikit (catalog no. 74104). First-strand cDNAs were synthesized using an RT^2 first-strand kit (catalog no. C-03; SABiosciences) following the manufacturer's protocol. The StepOnePlus real-time PCR system (Applied Biosystems) was used for the mouse mitochondrion-focused PCR array using RT^2 SYBR green/ROX qPCR master mix (catalog no. PA-012; SABiosciences) and an RT^2 Profiler PCR array kit (catalog no. PAMM-087C-2; SABiosciences). Quantitative real-time PCR analyses were performed with a Rotor-Gene RG3000 quantitative multiplex PCR instrument (Montreal Biotech Inc.) using Express SYBR green ER qPCR Super master mix (Invitrogen). Total cellular RNAs were isolated using TRIzol (Life Technologies) and then reverse transcribed using oligo(dT) primers and Moloney murine leukemia virus (M-MuLV) reverse transcriptase (New England Biotechnology).

RFP-MLN64 and filipin localization in mitochondria. RAW264.7 cells and TIR cells were cotransfected with RFP-MLN64 and GFP-BNIP3L plasmids. After 24 h, cells were plated on coverslips and treated with LeTx for 1 h. Cells were fixed with 3% formaldehyde for 1 h at room temperature. Formaldehyde was then quenched by incubating with glycine (1.5 mg/ml in PBS) at room temperature for 10 min. Cells were incubated with filipin (F-9765; 0.05 mg/ml in PBS–10% FBS; Sigma) for 2 h at room temperature and washed three times with PBS. Cells were visualized using multiphoton confocal microscope (LSM510 Meta; Zeiss), and images were taken under argon and helium-neon Chameleon lasers using ZEN software. For colocalization analysis, spatially calibrated images were analyzed using the "colocalization threshold" plugin of ImageJ 1.43u 64-bit software (National Institutes of Health, Bethesda, MD) with automatic thresholding and statistical significance testing for spatial intensity correlation analysis (18). Pearson's correlation coefficient of colocalized volumes measures the correlation between the intensities of the two labels in the colocalized voxels and is used to express the extent of colocalization, where a value of 1.0 represents perfect correlation.

Electron microscopy. Cells were grown on 14-cm dishes and incubated in the presence or absence of LeTx or ATP at 37°C in 5% CO_2. Cells were washed with PBS twice and fixed with 2.5% glutaraldehyde in a 0.1 M sodium cacodylate buffer for 2 h at room temperature. Grids with specimens were prepared according to the Transmission Electron Microscope Facility protocol at the University of Western Ontario (Canada), and micrographs were taken with a transmission electron microscope as previously described (27).

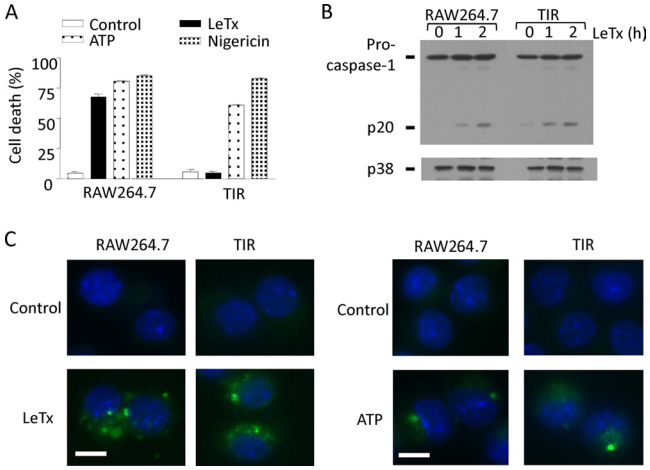

FIG 1 TIR cells are resistant to LeTx-induced pyroptotic events downstream of caspase-1 activation. (A) Wild-type (RAW264.7) and TIR cells were incubated in the presence or absence of LeTx (500 ng/ml LF and 1 μg/ml PA), ATP (5 mM), or nigericin (40 μM) for 5 h. Cell death was measured using MTT assay. Results are shown as the percentage of cell death compared with that in nontreated cells. Data are expressed as means and standard deviations (SD) ($n = 3$). (B) RAW264.7 and TIR cells were treated with LeTx (500 ng/ml LF and 1 μg/ml PA). Procaspase-1 and cleaved caspase-1 (p20) were measured by Western blotting. p38 blots were used as loading controls. (C) RAW264.7 and TIR cells were plated on coverslips and incubated in the absence or presence of LeTx (500 ng/ml LF and 1 μg/ml PA) or ATP (5 mM) for 2 h. Activation of caspase-1 was measured by the FLICA (fluorochrome inhibitor of caspase) system using a FAM-YVAD-FMK kit. Cells were labeled with FLICA as described in Materials and Methods. Cells were visualized at a magnification of ×600, and images were acquired using QCapture Pro software. Bar, 10 μm. Data are representative of more than three independent experiments.

Mitochondrial and late-endosome isolations. Mitochondrial and late-endosomal fractions were purified using a modified sucrose gradient method, as described in previous reports (6, 27). Briefly, cells were homogenized mechanically using a glass Dounce homogenizer in STE buffer (250 mM sucrose, 50 mM Tris, 1 mM EDTA, 1 mM NaF, 0.1 mM sodium orthovanadate, and protease inhibitor cocktail [pH 7.4]). The homogenates were centrifuged at 750 × g for 5 min to remove cell debris and nuclei, and supernatants were spun at 13,000 × g for 20 min to obtain mitochondrial pellets. Supernatants were further spun at 20,000 × g for 30 min to obtain the late-endosome fraction. All steps were performed on ice or at 4°C.

Cholesterol content measurements. Total cell lysates were prepared from 1.5 × 10^6 cells using RIPA buffer (50 mM Tris-HCl, 150 mM NaCl, 1 mM EDTA, 1× complete protease inhibitor [Roche], 1% Triton X-100, 0.1% sodium dodecyl sulfate [SDS] [pH 7.4]) as previously reported (26), and appropriate aliquots were used for protein quantification. Mitochondrial or late-endosome pellets prepared from 1.5 × 10^7 cells as described above were resuspended in hypotonic buffer containing 1% Triton X-100 and 0.1% SDS, and appropriate aliquots were used for protein quantification. Cholesterols in total cell lysates, mitochondrion-rich fractions, or late-endosome fractions were then extracted with chloroform-methanol (2:1, vol/vol) by the Folch method. After solvents evaporated, total cholesterols in the dried extract were quantified using an Amplex red cholesterol assay kit (A12216; Invitrogen, Molecular Probes) according to the manufacturer's protocol. Assay plates were read at an excitation of 544 nm and emission of 590 nm using a fluorometer (Fluoroskan Ascent FL; Thermo Scientific). Levels of cholesterol were calculated from fluores-

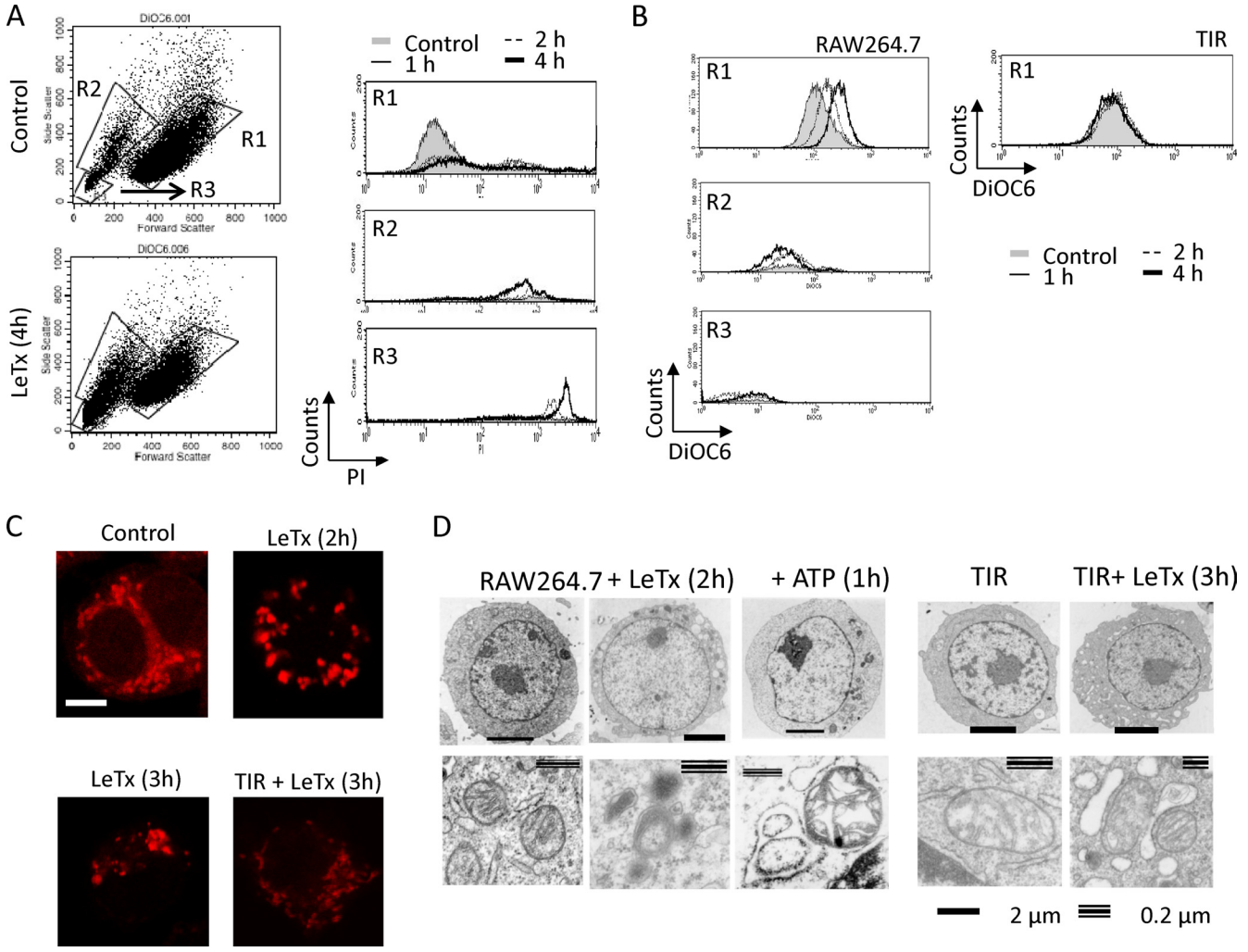

FIG 2 TIR cells are resistant to mitochondrial $\Delta\psi$ hyperpolarization induced by LeTx. (A and B) RAW264.7 cells were cultured in the presence or absence of LeTx (250 ng/ml LF and 500 ng/ml PA) for the times indicated. (A) Adherent cells were harvested and stained with propidium iodide. Cell death was analyzed by flow cytometry. (B) After cells were washed twice with prewarmed culture medium, adherent cells were stained with the mitochondrial fluorescent dye $DiOC_6$ to estimate mitochondrial membrane polarization and analyzed by flow cytometry. Data are representative of more than four independent experiments. (C) Cells were plated on coverslips and treated with LeTx (500 ng/ml LF and 1 μg/ml PA) for the indicated times. Cells were washed with prewarmed culture medium and stained with MitoTracker red as described in Materials and Methods. Cells were viewed by confocal microscopy (LSM510; Zeiss), and images were acquired using ZEN software. Bar, 5 μm. Images are representative of three independent experiments. (D) RAW264.7 and TIR cells were incubated in the absence or presence of LeTx (500 ng/ml LF and 1 μg/ml PA) or ATP (5 mM) for the indicated times, and cells were harvested and washed twice with ice-cold PBS. Cells were then fixed with 2.5% glutaraldehyde in 0.1 M sodium cacodylate buffer. Grids were prepared as described in Materials and Methods, and micrographs were taken with a transmission electron microscope.

cence (excitation, 540 nm; emission, 590 nm) values on the basis of a cholesterol reference standard.

GSH measurements. Mitochondrial fractions were prepared as described above and solubilized by suspending with 50 mM MES buffer [0.2 M 2-(*N*-morpholino)ethanesulfonic acid, 50 mM phosphate, and 1 mM EDTA (pH 6.0)] containing 1% Triton X-100. Small aliquots of the preparations were used for protein quantification. Samples were deproteinated by mixing with an equal volume of 10% (wt/vol) *meta*-phosphoric acid (no. 239275; Sigma-Aldrich) and treated with 4 M triethanolamine (TEAM; no. T58300; Sigma-Aldrich) to increase the pH of the samples. The TEAM treatment was carried out following the manufacturer's instructions (Cayman Chemical Company). To measure glutathione disulfide (GSSG) levels, free GSH was removed by treatment of 2-vinylpyridine (no. 13229-2; Sigma-Aldrich) from deproteinated samples. GSH contents were measured using a glutathione assay kit (no. 703002; Cayman Chemical Company) according to the manufacturer's instructions. Levels of total GSH or GSSG were calculated from absorbance (405 nm) values on the basis of a GSH or GSSG standard. For GSSG levels, standards were prepared similarly by adding 2-vinylpyridine followed by an incubation of the same duration as the sample.

RESULTS

TIR cells are specifically resistant to LeTx-induced pyroptosis, with no defects in activating caspase-1. Our previous study showed that a small population of LeTx-exposed cells (~2 to 4%) retains resistance to pyroptosis for more than 49 days (28). These toxin-induced resistant (TIR) cells were specifically resistant to LeTx but not to other pyroptosis-inducing agents, such as NLRP3-activating ATP or nigericin (Fig. 1A), and AIM2-activating poly(dA · dT) (see Fig. S1 in the supplemental material). TIR cells were shown to be normal in up taking LeTx (28); however,

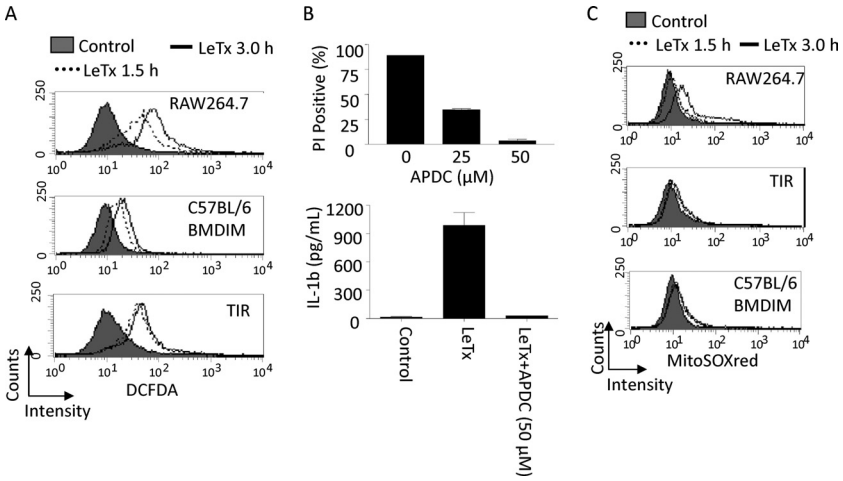

FIG 3 TIR cells are resistant to mitochondrial ROS production induced by LeTx. (A) Total cellular ROS productions was analyzed by flow cytometry using the ROS dye CM-H_2DCFDA (5 [and 6]-chloromethyl-2′,7′-dichlorodihydrofluorescein, acetyl ester; DCFDA) as described in Materials and Methods. RAW264.7, TIR, or C57BL/6 BMDIM cells were incubated in the presence or absence of LeTx (500 ng/ml LF and 1 μg/ml PA) for the indicated times and stained with 5 μM DCFDA. Data are representative of more than three independent experiments. (B) RAW264.7 cells were pretreated with APDC for 30 min and treated with LeTx (500 ng/ml LF and 1 μg/ml PA) in the absence or presence of APDC for 5 h. Cell death was measured by flow cytometry using PI staining, and data were analyzed using Cellquest software (top). Data are expressed as means and SD ($n = 3$). RAW264.7 cells were pretreated with LPS (1 μg/ml) for 4 h and incubated in the absence or presence of ammonium pyrrolidine dithiocarbamate (APDC; 50 μM) for 30 min. Cells were further cultured with or without LeTx (500 ng/ml LF and 1 μg/ml PA) for 2 h. Cell culture supernatants were collected and used for IL-1β measurement. Levels of IL-1β were quantified by ELISA using an eBioscience ELISA kit. Data are expressed as means and SD ($n = 3$). (C) RAW264.7, TIR, or BMDIM (C57BL/6) cells were treated with LeTx as described above and were washed with prewarmed culture medium. Cells were then stained with 2.5 μM Mitosox red as described in Materials and Methods. Mitochondrial ROS generation was analyzed by flow cytometry using Cellquest software. Data are representative of three independent experiments.

activation of caspase-1 by LeTx in these cells has not been examined. As shown in Fig. 1B and C, TIR cells showed no defects in cleaving procaspase-1 into caspase-1 and p20 (Fig. 1B) or in inducing the green fluorescence reporter specific for caspase-1 activity (Fig. 1C). Therefore, TIR cells likely gained resistance to LeTx/NLRP1b-induced pyroptosis by modifying downstream events of caspase-1 activation.

TIR cells are resistant to mitochondrial hyperpolarization induced by LeTx. Since LeTx causes mitochondrial dysfunction (3, 28), we investigated whether TIR cells were also susceptible to mitochondrial dysfunction induced by LeTx. To examine mitochondrial events in live cells, adherent macrophages were selected and examined through fluorescence-activated cell sorting (FACS) analysis. Floating cells were all PI positive, and the numbers were greatly increased as LeTx treatment continued (data not shown). Adherent cells showed three distinct patterns of forward and side scatter intensities (Fig. 2A, lower left). Cells in R1 were partially permeable for PI, and the permeability did not change through the LeTx treatments examined (Fig. 2A, upper right). In contrast, most cells in R2 were permeable to PI (Fig. 2A, middle right), and the numbers of R2 cells increased as LeTx treatment continued. The R3 population showed the highest intensities of PI (Fig. 2A, lower right) and most likely represented cell debris remaining from incomplete washes. Nontreated cells (control) also showed three distinct populations of forward and side scatter patterns, but >95% of cells were in the R1 area (Fig. 2A, upper left), and less than 5% of cells were floating (data not shown). The mitochondrial electron gradient across the membrane (mΔψ) was measured in these distinct cell populations using the mitochondrial fluorescent dye 3,3′-dihexyloxocarbocyanine iodide ($DiOC_6$), which accumulates in mitochondria in proportion to mΔψ. In R1 cells, mΔψ became more hyperpolarized as LeTx treatment continued, whereas R2 cells were hypopolarized and the number of R2 cells increased as LeTx treatment continued (Fig. 2B, left). These results suggest that LeTx caused hyperpolarization of mΔψ, followed by extensive hypopolarization, which almost coincided with the loss of plasma membrane integrity. LeTx-treated TIR cells showed neither hyperpolarization (Fig. 2B, right) in R1 nor hypopolarization in R2 (data not shown). Unlike LeTx, ATP and nigericin induced mΔψ hypopolarization without hyperpolarization in both wild-type and TIR cells (see Fig. S2 in the supplemental material). To further examine the morphology of mitochondria, LeTx-treated cells were visualized through confocal microscopy after staining of mitochondria with MitoTracker and electron microscopy. In nontreated (control) cells, mitochondria stained with MitoTracker were evenly scattered throughout the cytoplasm, whereas in LeTx-exposed cells, mitochondria became condensed and aggregated (Fig. 2C). Electron microscopy also showed shrunken and condensed mitochondria without apparent loss of plasma membrane integrity in LeTx-treated cells (Fig. 2D, left). LeTx-treated cells also exhibited multiple large low-density vacuoles. In contrast, ATP-treated cells contained swollen mitochondria with large vacuoles (Fig. 2D, middle). TIR cells also showed formation of large vacuoles in response to LeTx; however, no apparent changes were detected in mitochondrial structures (Fig. 2D, right). Collectively, these results suggest that LeTx caused mitochondrial hyperpolarization and condensation, which were distinct from ATP treatments, and that TIR cells were resistant to both mitochondrial hyperpolarization and condensation.

Generation of mitochondrial reactive oxygen species (ROS) is defective in TIR cells. ROS generation was shown to be required for NLRP3 and caspase-1 activation (20). LeTx was also shown to induce ROS generation in response to LeTx; however,

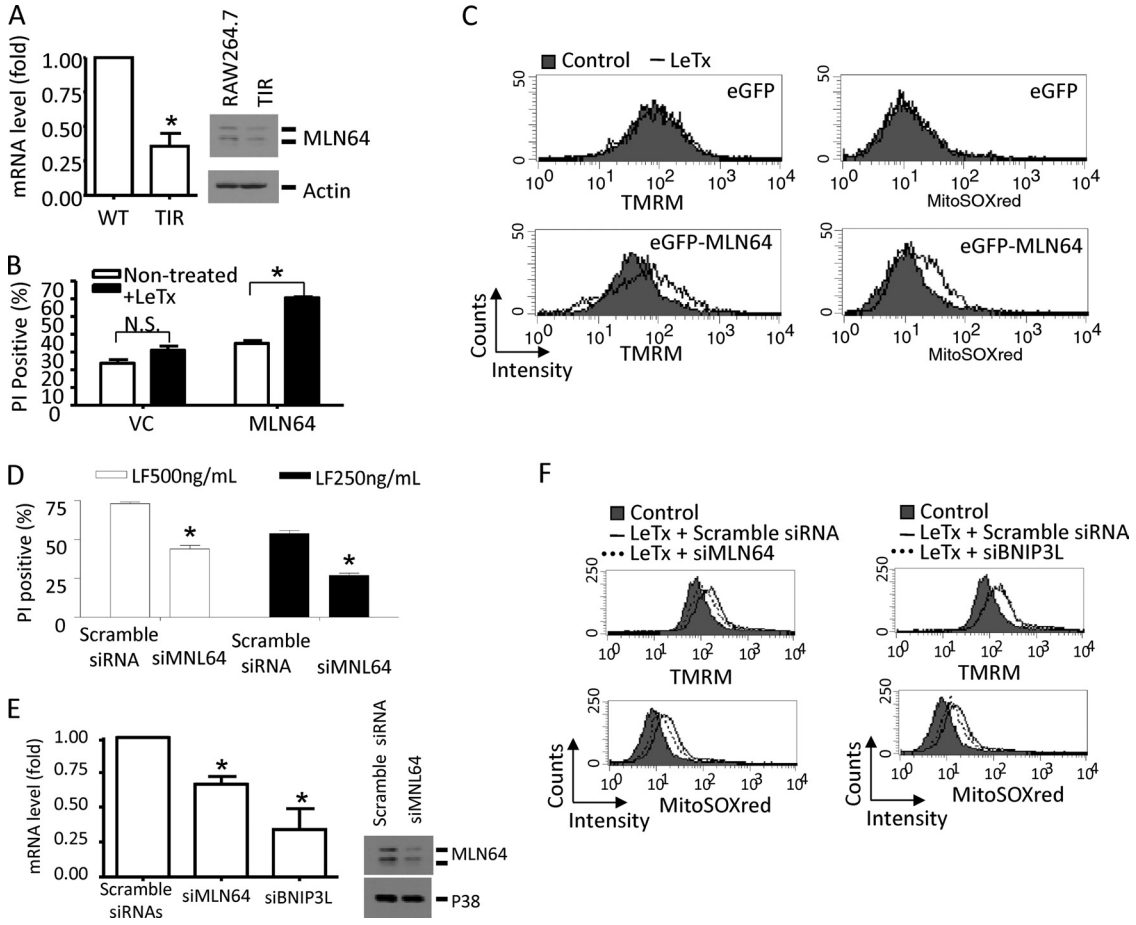

FIG 4 MLN64 expression is downregulated in TIR cells. (A) Total RNA was purified from RAW264.7 and TIR cells. cDNAs were synthesized, and expression levels of MLN64 mRNA were analyzed by quantitative real-time PCR (left). *, $P < 0.01$ (Student's *t* test). Protein levels of MLN64 in total cell lysates from RAW264.7 and TIR cells were analyzed by Western blotting using an antibody against the C terminus of MLN64 (right). (B and C) TIR cells were transfected with eGFP-labeled empty vector (VC) or eGFP-MLN64 plasmid (MLN64) using Lipofectamine 2000. (B) Twenty-four hours after transfection, TIR cells were treated with LeTx (500 ng/ml LF and 1 μg/ml PA) for 5 h, and cell death was measured by flow cytometry using PI staining. GFP-positive populations were used for cell death analysis. Data are expressed as means and SD ($n = 3$). N.S., not significant; *, $P < 0.05$. (C) Cells were treated with LeTx (500 ng/ml LF and 1 μg/ml PA) for 3 h, and mitochondrial membrane polarization was measured using a TMRM mitochondrial probe (left). Mitochondrial ROS production was also measured using Mitosox red (right). Data were acquired by flow cytometry using Cellquest software in GFP-positive cells as described in Materials and Methods. Data are representative of four independent experiments. (D) RAW264.7 cells were transfected with scrambled siRNA or mouse MLN64-specific siRNA (si-MLN64) as described in Materials and Methods. After 48 h transfection, cells were treated with LeTx (500 ng/ml LF or 250 ng/ml LF and 1 μg/ml PA) for 5 h, and cell death was measured by flow cytometry using PI staining. *, $P < 0.02$ (Student's *t* test). (E and F) MLN64 and BNIP3L were knocked down as described in Materials and Methods using siRNAs. After 48 h transfection, real-time PCR (E, left) and Western blotting (E, right) were performed. *, $P < 0.05$ (Student's *t* test). Cells were also treated with LeTx (500 ng/ml LF and 1 μg/ml PA) for 3 h, and mitochondrial membrane polarization (F, top) and mitochondrial ROS (F, bottom) were measured as described in Materials and Methods. Data are representative of three independent experiments.

its involvement in pyroptosis has been controversial (30, 55). We first examined whether ROS generation was required for LeTx-induced IL-1β production and pyroptosis. As previously shown, LeTx potently induced ROS generation as early as 90 min and maximally at 3 h after LeTx treatment (Fig. 3A, top). The antioxidant ammonium pyrrolidine dithiocarbamate (APDC) completely blocked LeTx-induced cell death and IL-1β production (Fig. 3B). To examine the role of NLRP1b in these cellular events, bone marrow-derived immortalized macrophages from C57BL/6 mice (C57BL/6 BMDIM) were treated with LeTx. These macrophages carry nonfunctional NLRP1b (11, 32) and were resistant to pyroptosis induced by LeTx (data not shown). In C57BL/6 BMDIM, ROS generation was also induced as early as 90 min (Fig. 3A, middle); however, peak generation at a later time was significantly diminished. TIR cells also showed a profile similar to that of C57BL/6 BMDIM, peaking at 1.5 h without further generation at 3 h (Fig. 3A, bottom). These data suggest that the sources of early and late ROS generation could be different: the earlier one was NLRP1b/caspase-1 independent, while the later one was NLRP1b/caspase-1 dependent. TIR cells were resistant to later ROS generation.

Since mΔψ hyperpolarization could trigger mitochondrial ROS generation (17, 33, 40), we examined mitochondrion-specific ROS generation in LeTx-treated cells using the mitochondrial ROS-specific dye Mitosox red. The dye accumulates in the mitochondria and exhibits red fluorescence after being oxidized by mitochondrial superoxide. LeTx induced red fluorescence mainly 3 h after LeTx treatments (Fig. 3C, top), whereas no red fluores-

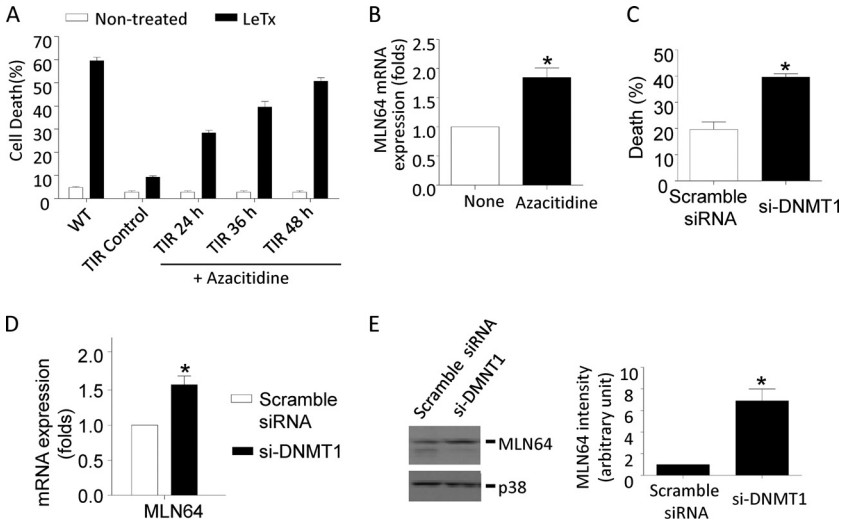

FIG 5 The DNMT inhibitor azacytidine and knockdown of DNMT1 by siRNAs render TIR cells sensitive to pyroptosis and enhance MLN64 expression. (A) TIR cells were cultured in the presence or absence of azacytidine (2 μM) for the indicated times. Nontreated RAW264.7 cells (WT), TIR cells, and TIR cells pretreated with azacytidine were exposed to LeTx (500 ng/ml LF and 1 μg/ml PA) for 5 h. Cell death was measured by MTT assay. (B) TIR cells were pretreated with azacytidine (2 μM) for 24 h, and MLN64 mRNA levels were analyzed by quantitative real-time PCR. (A and B) Data are expressed as means and SD ($n = 3$). *, $P < 0.05$ (Student's t test). (C to E) TIR cells were transfected with scrambled siRNA or mouse DNMT1-specific siRNA (si-DNMT1) for 48 h. (C) Cells were then treated with LeTx (500 ng/ml LF and 1 μg/ml PA) for 5 h, and cell death was measured by MTT assay. Data are expressed as means and SD ($n = 3$). *, $P < 0.05$ (Student's t test). (D) MLN64 mRNA expression levels were analyzed by quantitative real-time PCR. Data are expressed as means and SD ($n = 3$). *, $P < 0.05$ (Student's t test). (E) MLN64 expression was analyzed by Western blotting (left), and MLN64 immunoreactivity was analyzed using the NIH Image program (right). Data are expressed as means and SD ($n = 3$). *, $P < 0.05$ (Student's t test).

cence was detected even after 3-h treatments in both LeTx-treated TIR cells (Fig. 3C, middle) and C57BL/6 BMDIM (Fig. 3C, bottom). The lack of mitochondrial ROS generation in TIR cells could be contributed to by the high levels of superoxide dismutases, particularly mitochondrial superoxide dismutase (SOD2; also known as manganese superoxide dismutase). However, SOD2 expression levels were similar in both wild-type and TIR cells (see Fig. S3 in the supplemental material). These results suggest that TIR cells were resistant to NLRP1b-dependent mitochondrial ROS generation.

Down-regulation of MLN64 (metastatic lymph node 64) is involved in TIR. To identify mitochondrial genes involved in TIR, we performed quantitative RT-PCR-based PCR arrays (mouse mitochondrion RT^2 Profiler PCR array) targeting mRNAs corresponding to 84 genes in RAW264.7 and TIR cells. Among them, three genes were found to be downregulated more than 50% in TIR cells: Bcl2/adenovirus E1B 19-kDa interacting protein 3 (BNIP3), MLN64 (StARD3), and solute carrier family 25 (see Table S1 in the supplemental material). These findings confirm our previous report which showed downregulation of BNIP3 in TIR cells (28). The previous study also found BNIP3-like protein (BNIP3L) downregulation in TIR cells; however, the gene for this protein was not included in the array. MLN64 expression in TIR cells was further confirmed by gene-specific qPCR and Western blot analyses (Fig. 4A). To confirm its involvement in TIR, TIR cells were transfected with GFP-conjugated MLN64, and cell death, mΔψ, and mitochondrial ROS generation by LeTx were analyzed in GFP-positive cells. Overexpression of MLN64 rendered TIR cells more susceptible to cell death (Fig. 4B), mΔψ hyperpolarization, and mitochondrial ROS generation by LeTx (Fig. 4C). In these experiments, TMRM (tetramethylrhodamine methyl ester) instead of $DiOC_6$ was used as a fluorescent probe to monitor mΔψ, since TMRM does not interfere with green fluorescence and has low mitochondrial respiration-suppressive effects (52). In addition, knocking down MLN64 in RAW264.7 cells using small interfering RNA against MLN64 (si-MLN64) significantly lowered the degree of LeTx-induced cell death (Fig. 4D). RAW264.7 cells treated with si-MLN64 also partially prevented LeTx-induced mitochondrial ROS generation and mΔψ hyperpolarization (Fig. 4F). The incomplete inhibitory effects could be due to a partial suppression of MLN64 expression by si-MLN64 (Fig. 4E). Since we observed a better cell death-inhibitory effect by siRNAs targeting BNIP3L (si-BNIP3L) than BNIP3 (data not shown), BNIP3L was downregulated by si-BNIP3L in RAW264.7 cells, and mitochondrial ROS generation and mΔψ were measured in response to LeTx. Unlike in the case of MLN64, knocking down BNIP3L inhibited mitochondrial ROS generation but not hyperpolarization (Fig. 4F, right). Collectively, these results suggest that MLN64 was involved in mΔψ hyperpolarization and subsequent mitochondrial ROS generation, whereas BNIP3L was involved in ROS generation but not mΔψ hyperpolarization.

DNA methylation by DNMT1 is involved in MLN64 downregulation and TIR. We have previously shown that BNIP3 mRNA levels are quickly downregulated in LeTx-exposed cells due to the cleavage and inactivation of MAPKK and subsequent inactivation of p38 MAPK (28). However, the present study used TIR cells cultured 3 to 7 weeks after LeTx treatments and had normal basal activities of all MAPKs (data not shown). Therefore, downregulation of MLN64 in TIR cells was not likely mediated through inactivation of MAPKs by residual LF. Since TIR was sustained throughout multiple cell cycles, we examined if TIR was mediated by an epigenetic reprograming, particularly at the level of DNA methylation. Indeed, when TIR cells were treated with the broad-spectrum DNA methyltransferase inhibitor azacytidine,

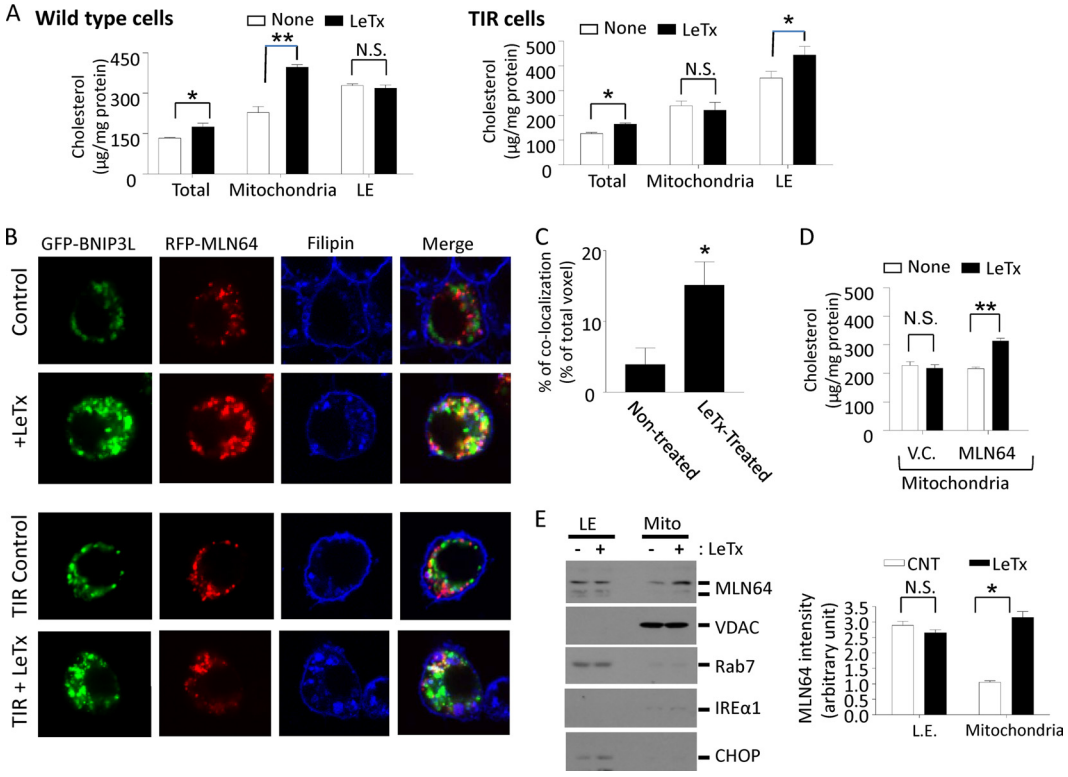

FIG 6 TIR cells are resistant to mitochondrial cholesterol accumulation induced by LeTx. (A) RAW264.7 cells and TIR cells were treated with LeTx (500 ng/ml LF and 1 μg/ml PA) for 1 h, and cells were washed and harvested. Mitochondrion- and late-endosome-rich fractions were isolated and cholesterol contents were measured as described in Materials and Methods. Data are expressed as means and SD ($n = 3$). Protein contents of RAW264.7 and TIR cells did not change as a result of LeTx treatments. N.S., not significant; *, $P < 0.1$; **, $P < 0.02$ (Student's t test). (B and C) RAW264.7 and TIR cells were transfected with GFP-BNIP3L and RFP-MLN64. After 24 h transfection, cells were treated with LeTx (500 ng/ml LF and 1 μg/ml PA) for 1 h. (B) Cells were fixed, stained with filipin, and observed by confocal microscopy (LSM510; Zeiss) as described in Materials and Methods. Images were acquired under argon and helium-neon Chameleon lasers using ZEN software. Images are representative of three independent experiments. (C) Colocalization of GFP-BNIP3L and filipin (blue) were measured using the NIH Image program for colocalization as described in Materials and Methods. *, $P < 0.05$ (Student's t test). (D) TIR cells were transfected with eGFP-labeled empty vector (V.C.) or eGFP-MLN64 plasmid (MLN64) for 24 h and were treated with LeTx (500 ng/ml LF and 1 μg/ml PA) for 1 h. Mitochondrion-rich fractions were isolated, and cholesterol contents were measured. Data are means and SD ($n = 3$). N.S., not significant; **, $P < 0.02$ (Student's t test). (E) RAW264.7 cells were treated with LeTx (500 ng/ml LF and 1 μg/ml PA) for 1 h, and mitochondrial and late-endosomal fractions were prepared as described in Materials and Methods. MLN64 translocation to mitochondria was estimated by Western blotting using an antibody against the C terminus of MLN64 (left). MLN64 immunoreactivities were analyzed using NIH Image program (right). Data are means and SD ($n = 3$). *, $P < 0.05$ (Student's t test).

TIR cells became sensitive to LeTx-induced pyroptosis in a time-dependent manner (Fig. 5A) and transcript levels of MLN64 were increased (Fig. 5B). Furthermore, knocking down DNA methyltransferase 1 (DNMT1) by siRNA (si-DNMT1) to about 50% (see Fig. S4 in the supplemental material) rendered TIR cells sensitive to LeTx-induced pyroptosis (Fig. 5C) and significantly induced MLN64 expression in TIR cells (Fig. 5D and E). These results suggest that downregulation of MLN64 in TIR cells is at least in part mediated through DNA methylation at genomic levels.

TIR cells are resistant to LeTx-induced mitochondrial cholesterol accumulation. MLN64 is a late-endosomal protein shown to be involved in transferring cholesterol from endolysosomal compartments to the mitochondrial inner membrane (14). Therefore, we examined cholesterol accumulation in mitochondrial membranes using the Amplex red cholesterol assay kit, which measures both free cholesterol and cholesteryl esters. Indeed, mitochondrial fractions from RAW 264.7 cells treated with LeTx contained significantly higher concentrations of cholesterol than those from nontreated cells (Fig. 6A, left). However, in TIR cells, an increase in late-endosomal but not mitochondrial cholesterol contents was detected in TIR cells (Fig. 6A, right panel). There was a small but significant increase in total cholesterol contents in both wild-type and TIR cells. Thus, it is possible that an overall increase in total cholesterol contents was due at least in part to an increase in mitochondrial and late-endosomal cholesterol contents in wild-type cells and TIR cells, respectively. Cholesterol accumulation was also visualized using filipin after transfection of cells with both GFP-BNIP3L and RFP-MLN64 to monitor their localization with mitochondrial and MLN64-positive compartments, respectively. In nontreated cells, BNIP3L (mitochondrion)- and MLN64-positive puncta were rarely colocalized, and filipin-positive puncta were in part colocalized with MLN64-positive but rarely with BNIP3L-positive compartments (Fig. 6B, top row). LeTx-treated cells, however, exhibited highly aggregated mitochondria colocalized with MLN64-positive and filipin-positive compartments (Fig. 6B, second row). TIR cells reconstituted with BNIP3L and MLN64 showed similar colocalization patterns in response to LeTx treatments (Fig. 6B, third and bottom rows). Quantitative colocalization analyses also indicated that BNIP3L- and filipin-positive puncta were colocalized at sig-

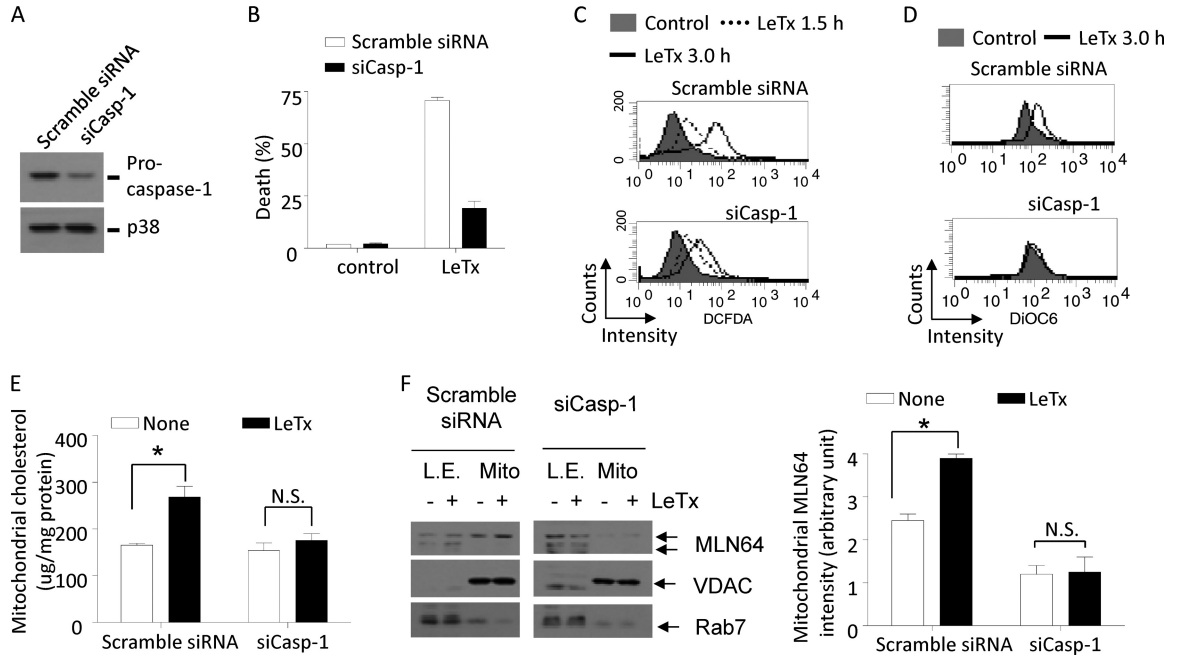

FIG 7 LeTx causes caspase-1-dependent mΔψ hyperpolarization, and mitochondrial MLN64 and cholesterol accumulation. (A to F) RAW264.7 cells were transfected with scrambled siRNA or mouse caspase-1-specific siRNA (siCasp-1) using Lipofectamine RNAi MAX (Invitrogen) for 40 h. Procaspase-1 protein levels were analyzed by Western blotting (A) and cell death by MTT assays after treatment of cells with LeTx (500 ng/ml LF and 1 μg/ml PA) for 5 h (B). Data are expressed as means and SD ($n = 3$). (C) RAW264.7 cells transfected with scrambled siRNA or siCasp-1 were incubated with LeTx (500 ng/ml LF and 1 μg/ml PA) for the indicated times, and total ROS generation was measured by flow cytometry using CM-H_2DCFDA dye. Data are representative of two independent experiments. (D) Cells were treated with LeTx (500 ng/ml LF and 1 μg/ml PA) for 3 h, and mitochondrial membrane polarization was measured as described in Materials and Methods. Data are representative of three independent experiments. (E and F) Cells were treated with LeTx (500 ng/ml LF and 1 μg/ml PA) for 1 h. Mitochondrion- and late-endosome-rich fractions were isolated and cholesterol contents were measured as described in Materials and Methods. *, $P < 0.05$ (Student's t test); N.S., not significant. (F) MLN64 translocation into mitochondria was estimated by Western blotting (left), and MLN64 immunoreactivities in mitochondria were analyzed using the NIH Image program (right). Data are expressed as means and SD ($n = 3$). *, $P < 0.05$ (Student's t test); N.S., not significant.

nificantly higher levels in LeTx-exposed cells (~16%) than in nontreated wild-type cells (~3.5%) (Fig. 6C). In line with these results, TIR cells overexpressing MLN64 showed increased mitochondrial cholesterol levels in response to LeTx (Fig. 6D). We then examined whether LeTx induced the translocation of MLN64 from late endosomes to mitochondria by Western blotting on endosomal and mitochondrial fractions. As shown in Fig. 6E, significantly higher MLN64 immunoreactivities were detected in mitochondrial fractions of LeTx-treated cells than nontreated cells. Western blots against the mitochondrial voltage-dependent anion channel (VDAC), the late-endosomal protein Rab7, and the endoplasmic reticulum proteins IREα1 and CHOP showed little cross contamination and equal levels of sample loading.

Mitochondrial dysfunction and MLN64 translocation by LeTx are mediated by caspase-1. Next, we examined whether caspase-1 was required for mitochondrial ROS generation, cholesterol accumulation, and MLN64 translocation by LeTx. RAW264.7 cells treated with siRNAs targeting procaspase-1 (siCasp-1) showed more than a 70% downregulation of procaspase-1 expression relative to nontreated cells (Fig. 7A) and were significantly resistant to LeTx-induced pyroptosis (Fig. 7B). Also, these cells were resistant to the later total ROS generation (Fig. 7C) and mitochondrial hyperpolarization (Fig. 7D) compared with scrambled siRNA-treated cells. Similarly, knocking down procaspase-1 suppressed mitochondrial cholesterol (Fig. 7E) and MLN64 accumulation (Fig. 7F) in response to LeTx. Therefore, these results collectively suggest that caspase-1 plays a crucial role in MLN64-mediated mitochondrial dysfunction induced by LeTx.

M-β-CD treatment prevents mitochondrial cholesterol accumulation, mΔψ hyperpolarization, mitochondrial ROS generation, and cell death. To further examine the role of mitochondrial cholesterol accumulation in LeTx cytotoxicity, methyl-β-cyclodextrin (M-β-CD) was used to deplete cholesterol in late endosomes and lysosomes. M-β-CD is a cyclic oligosaccharide that dissolves lipids in its hydrophobic core (31). It is taken up through an endocytic pathway and reduces cholesterol storage by acting from inside endocytic organelles such as late endosomes and lysosomes (49). M-β-CD treatments at 5 mM for 18 h slightly decreased total cellular and mitochondrial cholesterol levels in non-LeTx-treated cells; moreover, mitochondrial cholesterol accumulation by LeTx was almost completely abolished by M-β-CD (Fig. 8A). LeTx-induced mitochondrial ROS production (Fig. 8B), mΔψ hyperpolarization (Fig. 8C), and cell death (Fig. 8D) were also suppressed by M-β-CD treatment. M-β-CD at the concentration used was nontoxic to RAW264.7 cells (data not shown) and had no effects on LeTx entry, as demonstrated by normal MEK1 and caspase-1 cleavage by LF (see Fig. 5S in the supplemental material). These results, together with the effects of si-MLN64 (Fig. 4 and 6), suggest that mitochondrial cholesterol enrichment by LeTx is involved in both mΔψ hyperpolarization and mitochondrial ROS generation.

Mitochondrial cholesterol accumulation leads to the depletion of mitochondrial glutathione and the generation of ROS. Under normal conditions, 1 to 2% of the oxygen in mitochondria

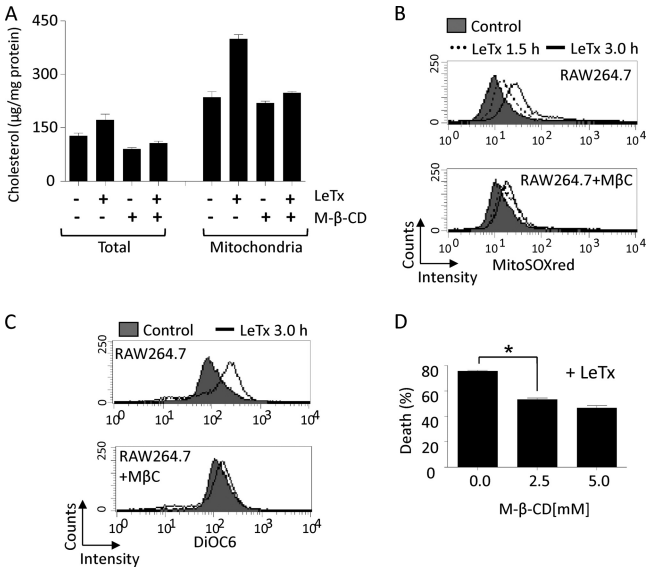

FIG 8 Methyl-β-cyclodextrin (M-β-CD) inhibits mitochondrial cholesterol accumulation, mitochondrial hyperpolarization, mitochondrial ROS generation and cell death induced by LeTx. (A to C) RAW264.7 cells were cultured with or without M-β-CD (5.0 mM) for 18 h and further cultured with LeTx (500 ng/ml LF and 1 μg/ml PA) for additional 1 h. (A) Total lysates or mitochondrion-rich fractions were prepared and cholesterol contents in those samples were measured as described in Materials and Methods. Data are expressed as means and SD ($n = 3$). (B and C) RAW264.7 cells were pretreated with M-β-CD (5.0 mM) for 18 h and further incubated with LeTx (500 ng/ml LF and 1 μg/ml PA) for the indicated times. Mitochondrial ROS generation and mitochondrial membrane polarization were measured by flow cytometry using Mitosox red probe (B) or $DiOC_6$ (C). Data are representative of three independent experiments. (D) RAW264.7 cells were pretreated with M-β-CD (2.5 mM, 5.0 mM) for 18 h and further incubated with LeTx (500 ng/ml LF and 1 μg/ml PA) for 5 h. Cell death was measured by MTT assay. Data are expressed as means ± SD ($n = 3$). *, $P < 0.05$ (Student's t test).

is reduced to generate ROS during respiration processes (44), and glutathione (GSH) plays an important role in detoxifying ROS (46). All mitochondrial GSH is transported from the cytoplasm by specific anion carriers, whose activities can be hampered by cholesterol enrichment in the mitochondrial membrane (21, 24). Since cholesterol accumulated in the mitochondrial membrane upon LeTx treatments (Fig. 6), we examined mitochondrial amounts of total GSH, including both free GSH and its oxidized form, glutathione disulfide (GSSG). As shown in Fig. 9A, LeTx caused a gradual decrease in total GSH levels in wild-type cells, whereas in TIR cells the amounts did not change. The ratio of GSSG to GSH was also greatly increased by LeTx treatment in wild-type but not TIR cells (Fig. 9B). These results suggest that LeTx caused a general reduction of mitochondrial total and free GSH levels in wild-type but not TIR cells.

mΔψ hyperpolarization causes mitochondrial ROS generation. Mitochondria contain several glutathione *S*-transferases (GSTs), which play an important role in detoxifying oxidative damages through GSH conjugation and peroxidase activity. Among them, the mitochondrial inner membrane-associated GST isoform A4 (GSTA4) was particularly shown to have a high peroxidase activity and to protect cells from mitochondrial oxidative stress and cell death (5, 16, 67). Thus, we examined the effects of GSTA4 overexpression in LeTx-induced mitochondrial dysfunction and cell death. RAW264.7 cells transfected with either eGFP empty vector or eGFP-conjugated GSTA4 vector were exposed to LeTx, and mΔψ hyperpolarization, mitochondrial ROS generation, and cell death were measured in GFP-positive cells using FACS. Overexpression of GSTA4 decreased mitochondrial ROS contents (Fig. 9C, bottom) and modestly but significantly prevented cell death by LeTx (Fig. 9D); however, mΔψ hyperpolarization was not affected (Fig. 9C, top). These results, together with the findings shown in Fig. 4C and F, suggest that mΔψ hyperpolarization preceded mitochondrial ROS generation and cell death.

Mitochondrial ROS generation from the electron transport chain causes cell death induced by LeTx. The mitochondrial electron transport chain (ETC) maintains mΔψ and is the major source of mitochondrial ROS generation. To examine whether the ETC was responsible for mΔψ hyperpolarization in LeTx-treated cells, RAW264.7 cells were treated with various chemical inhibitors targeting mitochondrial ETC complexes (15), and mΔψ hyperpolarization and mitochondrial ROS production by LeTx was measured in R1 population cells, as described in the legend to Fig. 2A. All the ETC inhibitors examined, including diphenyleneiodonium (DPI; a broad-spectrum NADPH oxidase inhibitor which inhibits both microsomal and mitochondrial [ETC complex I] NADPH oxidase), rotenone (a mitochondrial ETC complex I inhibitor), and antimycin A (a mitochondrial ETC complex III inhibitor), substantially prevented both mΔψ hyperpolarization and mitochondrial ROS production induced by LeTx (Fig. 10A). However, these inhibitors caused more extensive overall mΔψ hypopolarization alone (see Fig. S6 in the supplemental material), and more extensive cell death together with LeTx (data not shown). In fact, NADPH inhibitors were shown to cause extensive hypopolarization, which in turn results in ROS production and cell death (38, 66).

We then examined the effects of mitochondrion-specific ROS scavengers apocynin and Mito-Tempo on mΔψ hyperpolarization induced by LeTx. As shown in Fig. 10B, both scavengers substantially decreased mitochondrial ROS generation without influencing mΔψ hyperpolarization in LeTx-treated cells. These mitochondrion-specific scavengers significantly suppressed LeTx-induced cell death (Fig. 10C). These results, together with other results obtained here (Fig. 4F and 9C), suggest that mΔψ hyperpolarization preceded ROS generation, which caused cell death in response to LeTx.

Bone marrow-derived primary macrophages show features of mitochondrial dysfunction similar to those of immortalized macrophages. To further examine the involvement of MLN64 in LeTx-induced pyroptosis in cells other than immortalized macrophages, primary bone marrow-derived macrophages from 129/S1 and DBA/2J strains of mice were exposed to LeTx. As expected, macrophages from 129/S1 mice harboring functional NLRP1b were sensitive to LeTx-induced pyroptosis, whereas DBA/2J macrophages lacking NLRP1b were resistant (Fig. 11A). Macrophages from 129/S1 also showed similar mitochondrial defects as observed in RAW264.7 cells, including mΔψ hyperpolarization (Fig. 11B), and mitochondrial accumulation of cholesterol (Fig. 11C) and MLN64 (Fig. 11D). These mitochondrial changes were not detected in DBA/2J macrophages, suggesting that LeTx also causes MLN64-mediated mitochondrial dysfunction in primary macrophages harboring functional NLRP1b.

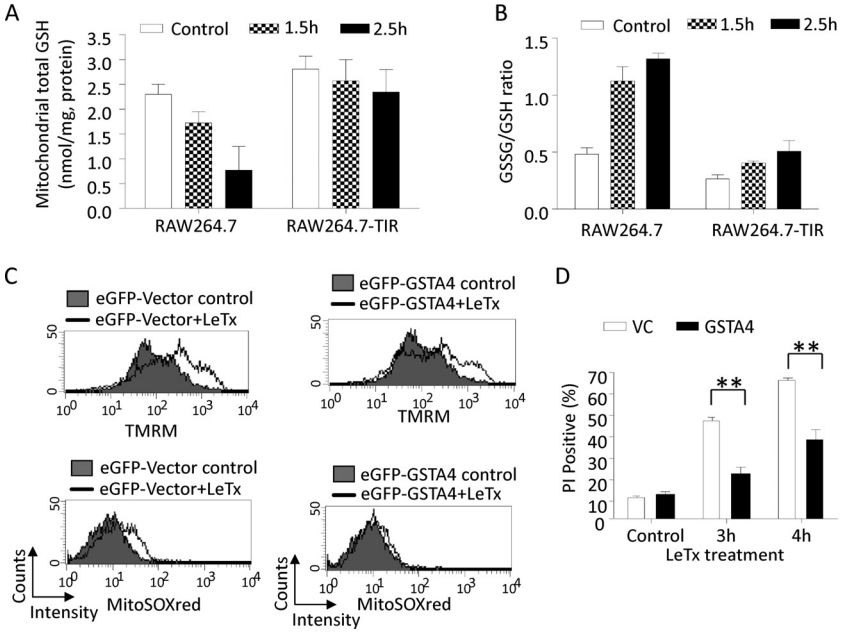

FIG 9 Mitochondrial cholesterol accumulation leads to a depletion of mitochondrial glutathione and a generation of mitochondrial ROS. (A and B) RAW264.7 cells and TIR cells were treated with LeTx (500 ng/ml LF and 1 μg/ml PA) for the indicated times. After two washes with PBS, mitochondrial fractions were prepared and levels of GSH (A) and GSSG (B) were measured as described in Materials and Methods. Data are expressed as means and SD ($n = 2$ [A and B]). (C and D) RAW264.7 cells were transfected with eGFP-labeled empty vector (VC) or eGFP-GSTA4 plasmid. After 24 h of incubation, cells were treated with LeTx (500 ng/ml LF and 1 μg/ml PA) for 3 h, and mitochondrial membrane potential (top) and mitochondrial ROS (bottom) in GFP-positive populations were measured by flow cytometry as described in Materials and Methods. Data are representative of three independent experiments. (D) RAW264.7 cells transfected with eGFP-labeled empty vector (VC) or eGFP-GSTA4 were treated with LeTx (500 ng/ml LF and 1 μg/ml PA) for the indicated times. Cells positive for both GFP and PI were analyzed by flow cytometry using Cellquest software. $n = 3$; **, $P < 0.01$ (Student's t test).

DISCUSSION

Caspase-1 plays an integral role in inflammasome-induced pyroptosis. However, the mechanism by which caspase-1 induces pyroptosis is largely unknown. Here we show that LeTx/NLRP1b also induces pyroptosis by activating caspase-1 but has features of mitochondrial dysfunction distinct from those of NLRP3 and AIM2 (Fig. 2 and 7; also, see Fig. S1 in the supplemental material). Caspase-1 was shown to target different substrates depending on the type of inflammasome activation (2); therefore, different characteristics in cell death by different inflammasomes are not surprising. Also, LF could have targeted MAPKKs and unknown targets that contributed to the unique mitochondrial features. In addition, the source and requirement of ROS in NLRP1b for inflammasome activation appeared to be distinct from those in NLRP3. It was previously shown that mitochondrial ROS generation is a prerequisite for NLRP3 activation (66). Similarly, the ROS scavenger APDC completely inhibited LeTx-induced caspase-1 activation (Fig. 3B), and ROS generation was detected in cells deficient in NLRP1b (Fig. 3A), suggesting that ROS was generated before NLRP1b/caspase-1 activation. However, unlike with NLRP3, mitochondrial ROS generation was detected only after initial ROS generation (~3 h after LeTx treatment) (Fig. 3C) and was not detected in TIR, NLRP1b-deficient (Fig. 3C), and caspase-1 knockdown (Fig. 7D) cells. The source of the initial ROS is not clear. The membrane-associated Nox/Duox family NADPH oxidases have been shown to be involved in inflammasome activation (20, 25, 42). However, how LeTx induces nonmitochondrial ROS generation and what NOX complexes are responsible for the generation are still to be investigated. Overall, this study suggests that although caspase-1 is a common requirement for all known pyroptosis, its features in cell death can vary with different stimuli.

Among the 84 genes known to be associated with mitochondrial dysfunction, MLN64 was substantially (>50%) downregulated in TIR cells. Here, we showed that the downregulation of MLN64 in TIR cells was at least in part through a DNMT1-mediated epigenetic reprograming at the level of DNA methylation (Fig. 5). Previously, LeTx was shown to induce epigenetic reprograming through histone modifications, including inhibition of histone H3 phosphorylation at Ser 10 that caused suppression of IL-18 production (45). LeTx also induces expression of the jumonji C family histone 3 lysine-27 (H3K27) demethylase 3, which was correlated with toxin resistance (19). However, the direct linkage between these histone modifications and TIR are yet to be established. We here show that DNA methylation, which is mediated at least in part by DNMT1, is required for maintaining TIR phenotypes (Fig. 5). Since DNA methylation causes gene suppression, downregulation of MLN64 through increased methylation at genomic levels is a reasonable proposition. However, further studies are required to determine whether an increase of DNA methylation by LeTx is caused by histone modifications, and whether MLN64 expression is directly regulated by DNA methylation at its genomic region.

MLN64, also known as the steroidogenic acute regulatory-related (StAR) lipid transfer protein 3, is a member of the StAR-related lipid transfer domain (StARD)-containing protein family, which is expressed mainly in steroidogenic tissues. Among the 15 mammalian StARD-containing proteins, MLN64 was shown to be

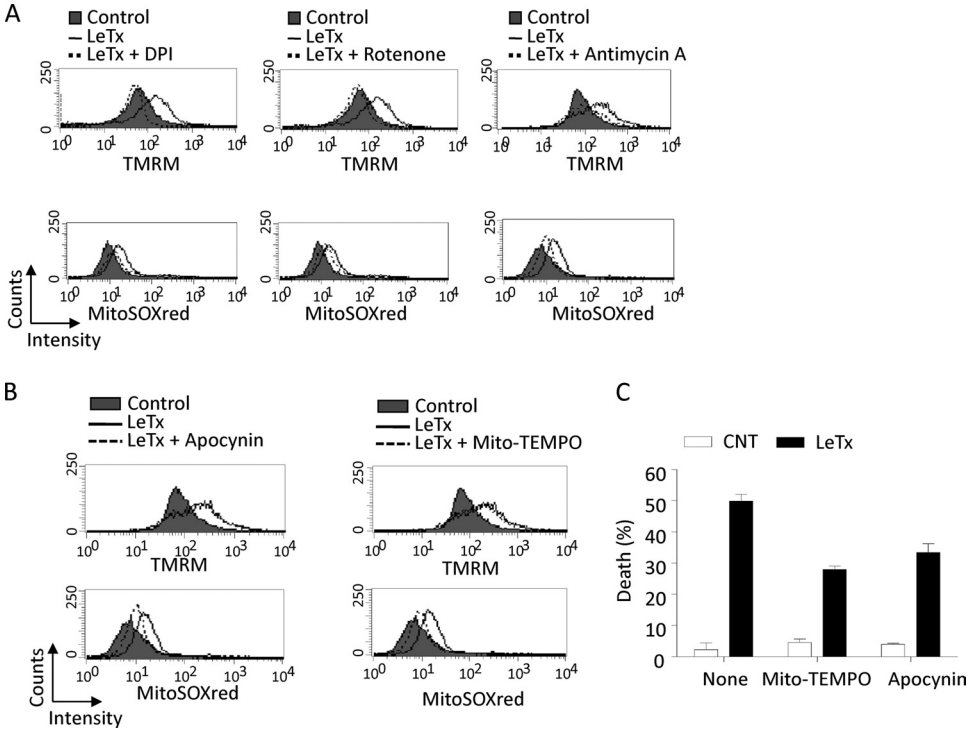

FIG 10 mΔψ hyperpolarization-dependent mitochondrial ROS generation is involved in death induced by LeTx. (A) RAW264.7 cells were pretreated with DPI (2 μM), rotenone (1 μM), or antimycin A (10 μg/ml) for 1 h and further incubated with or without LeTx (500 ng/ml LF and 1 μg/ml PA) or LeTx plus inhibitors for 3 h. Cells were then washed with prewarmed culture medium and stained with TMRM (top) or Mitosox red (bottom) as described in Materials and Methods. Data are representative of four independent experiments. (B) RAW264.7 cells were pretreated with apocynin (0.5 mM) or Mito-Tempo (10 μM) for 1 h and treated with LeTx as described above (A). Cells were stained with TMRM (top) or Mitosox red (bottom) as described in Materials and Methods. Data are representative of three independent experiments. (C) Cells were preincubated as for panels A and B and incubated with LeTx (250 ng/ml LF and 500 μg/ml PA) for 5 h. Cell death was measured by MTT assay, and data are expressed as means ± SD ($n = 3$).

expressed in all tissues (56, 63) and involved in transferring cholesterol from the endolysosomal membrane to the mitochondrial membrane (14, 47, 65). The N-terminal transmembrane domain called MENTAL (MLN64 N-terminal) targets MLN64 mainly to late endosomes (4, 47), and the C-terminal StARD is involved in translocation of MLN64 to mitochondria. Since the MENTAL domain also binds cholesterol, it was suggested that MLN64 captures cholesterol in the endolysosomal compartment and the cytoplasmic StARD then transfers the cholesterol to the mitochondria through interacting with the translocator protein (36, 48). Although it is not clear how MLN64 trafficking or expression is regulated under pathogenic conditions, the involvement of MLN64 and mitochondrial cholesterol load in cell death has been demonstrated. For example, overexpression of MLN64 caused cell death in hepatocytes and CHO cells (60), and mitochondrial cholesterol load sensitizes cells to amyloid β peptide- and tumor necrosis factor-induced cell death (9, 41). In line with these studies, we first showed that MLN64 trafficking to mitochondria was enhanced by LeTx (Fig. 6E), resulting in increased cholesterol load in mitochondria (Fig. 6A). TIR cells that were resistant to mitochondrial cholesterol load became sensitive after MLN64 overexpression, supporting that downregulation of MLN64 was a main adaptation to mitochondrial cholesterol load by LeTx in TIR cells. It is still not clear how LeTx caused translocation of MLN64 to mitochondria. At least it appeared that mitochondrial translocation of MLN64 was downstream of caspase-1 activation, since LeTx did not cause mitochondrial translocation of MLN64 in NLRP1b-deficient C57BL/6 BMDIM (data not shown), and reconstitution of MLN64 in TIR cells reinstated mΔψ hyperpolarization and mitochondrial ROS generation, which was dependent on NLRP1b and caspase-1 (Fig. 3 and 7). It has been suggested that the StARD could be released by a proteolytic process, leading to mitochondrial localization (65). Several studies have looked into substrates targeted by caspase-1 (2, 35, 53); however, MLN64 was not identified as a caspase-1 substrate. We also did not detect any changes in the levels of cleaved MLN64 in the presence of LeTx (data not shown), ruling out the possibility of MLN64 as a LF or caspase-1 substrate. In fact, it was suggested that pyroptosis involves an inflammasome formation distinct from IL-1β process, which does not require autoproteolytic activation of caspase-1 (12). TIR cells had no defects in processing procaspase-1 (Fig. 1), and knocking down caspase-1 by siRNA almost completely prevented cell death (Fig. 7), but prevention of cell death by the caspase-1 inhibitor Ac-YVAD-CMK, even at the highest dose used, was minimal (data not shown). As previously documented (64), the minimal protection of cell death by the inhibitor could also have been due to their inability in complete inhibition of caspase-1 activation. Thus, whether TIR cells are defective in forming an inflammasome (cleavage independent) in addition to MLN64 downregulation remains to be investigated.

Mitochondria should have a stable mΔψ and redox transitions to maintain their function and integrity. Various pathological conditions have shown to cause both hyper- and hypopolarizations of mΔψ, resulting in excess mitochondrial ROS production (10, 34).

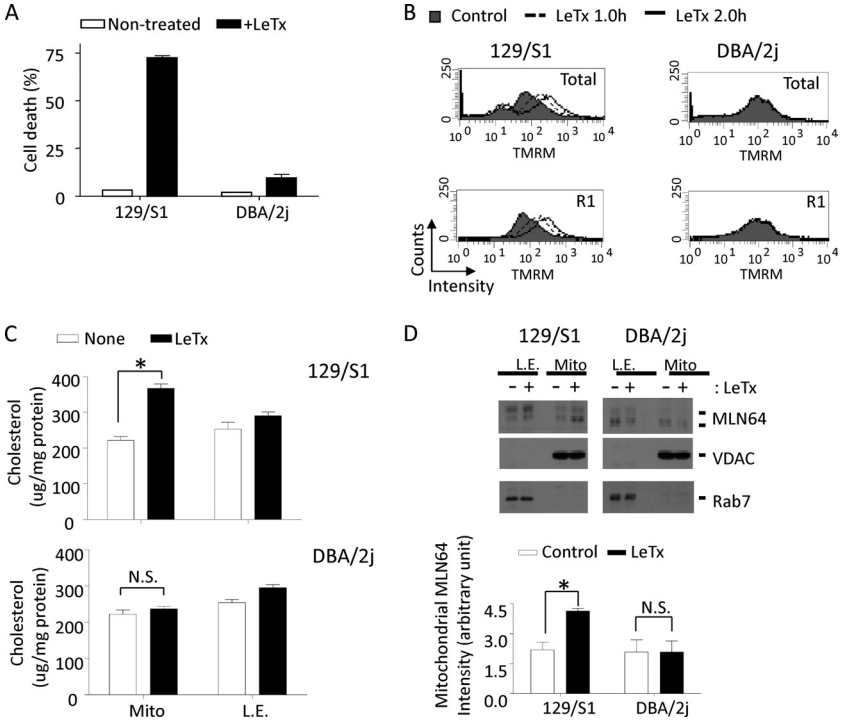

FIG 11 Mitochondrial hyperpolarization, cholesterol and MLN64 accumulation, and cell death by LeTx in bone marrow-derived primary macrophages (BMDMs). (A) BMDMs prepared from 129/S1 or DBA/2J mice were treated with LeTx (500 ng/ml LF and 1 μg/ml PA) for 2.5 h, and cell death was measured by MTT assay. Data are means and SD ($n = 3$). (B) BMDMs were treated with LeTx (500 ng/ml LF and 1 μg/ml PA) for the indicated times, and mitochondrial membrane potential was measured as described in Materials and Methods. Data are representative of three independent experiments. (C and D) BMDMs from 129/S1 or DBA/2J mice were incubated with LeTx (500 ng/ml LF and 1 μg/ml PA) for 1 h. (C) Mitochondrion-rich fractions were isolated and cholesterol contents were measured as described in Materials and Methods ($n = 3$; *, $P < 0.05$; N.S., not significant). (D) Mitochondrial or late-endosome fractions were isolated, and then levels of MLN64 were analyzed by Western blotting (top) and immunoactivities for MLN64 in mitochondria were analyzed using NIH-image program (bottom). *, $P < 0.05$ (Student's t test); N.S., not significant ($n = 3$).

Here we showed that TIR cells were resistant to LeTx-induced mΔψ hyperpolarization through downregulating MLN64 expression (Fig. 4A to C) and in turn preventing mitochondrial cholesterol load (Fig. 6A and B). Since mΔψ is regulated by the activity of the electron transport chain, it is possible that mitochondrial membrane rigidity due to increased cholesterol load caused a transient hyperpolarization before overwhelming hypopolarization. This notion is also supported by the findings that depletion of late-endosomal/lysosomal cholesterol by M-β-C prevented mΔψ hyperpolarization (Fig. 8C). In addition, LeTx was shown to rapidly upregulate proteins involved in mitochondrial ATP generation in macrophages, including RAW264.7 and J774A.1 cells (13, 51), which could have contributed mΔψ hyperpolarization.

Mitochondrial cholesterol load has been shown to deplete mitochondrial GSH contents by altering GSH transporting carrier activities (21, 24) and to facilitate the cell death process (22, 41). Similarly, here we showed that LeTx caused depletion of both total and free GSH contents in mitochondria, likely due to cholesterol accumulation in mitochondrial membranes (Fig. 6). Indeed, overexpression of GSTA4, a mitochondrial GST with high peroxidase activity (5), in RAW264.7 cells substantially prevented mitochondrial ROS generation and cell death by LeTx but not mΔψ hyperpolarization (Fig. 9C and D). Therefore, it appears that MLN64-mediated mitochondrial cholesterol enrichment caused mitochondrial dysfunction by aggravating ROS generation by mΔψ hyperpolarization and rendering mitochondria vulnerable to ROS-induced damage by depletion of ROS scavenging capacity.

Different types of cells have different adaptations to stresses, related to their survival and function. For example, neuronal cells and cardiomyocytes exposed to a brief ischemia/reperfusion adapt to such stresses and become resistant to subsequent lethal ischemia/reperfusion challenges. In macrophages, cellular adaptations to different toxins, including lipopolysaccharide and LeTx, have been demonstrated in cytokine production and pyroptotic cell death, respectively. Detection of microbial components by Toll-like receptors is a key aspect of innate immunity in sensing invading microbes. Similarly, activation of NLRP1b by LeTx was shown to be beneficial to the host in fending off *Bacillus anthracis* spore infection through releasing the inflammatory cytokines IL-1β and IL-18 (43, 59). However, LeTx was also shown to be required for the dissemination of bacteria beyond the draining lymphoid tissue (39), which could be mediated through pyroptosis. Therefore, whether the adaptive response of macrophages to pyroptosis is beneficial for the host in anthrax infection is still to be investigated. Various bacterial pathogens actively induce rapid host cell death as a mechanism to destroy host immune cells and facilitate early dissemination, and overactive inflammasome activation and pyroptosis have been shown to be involved in various inflammatory diseases (58). The mechanism of mitochondrial dysfunction induced in a caspase-1-dependent manner described in this study constitutes a new means of regulating the process of pyroptosis, which can be targeted for novel therapeutics in treating such diseases.

ACKNOWLEDGMENTS

This work was supported by a Canadian Institute of Health Research Operating Grant (MOP93551) to S.O.K.

We thank Macon Coleman for editing the manuscript.

REFERENCES

1. **Adami C, Brunda MJ, Palleroni AV.** 1993. In vivo immortalization of murine peritoneal macrophages: a new rapid and efficient method for obtaining macrophage cell lines. J. Leukoc. Biol. **53**:475–478.
2. **Agard NJ, Maltby D, Wells JA.** 2010. Inflammatory stimuli regulate caspase substrate profiles. Mol. Cell. Proteomics **9**:880–893.
3. **Alileche A, Squires RC, Muehlbauer SM, Lisanti MP, Brojatsch J.** 2006. Mitochondrial impairment is a critical event in anthrax lethal toxin-induced cytolysis of murine macrophages. Cell Cycle **5**:100–106.
4. **Alpy F, Tomasetto C.** 2006. MLN64 and MENTHO, two mediators of endosomal cholesterol transport. Biochem. Soc. Trans. **34**:343–345.
5. **Aniya Y, Imaizumi N.** 2011. Mitochondrial glutathione transferases involving a new function for membrane permeability transition pore regulation. Drug Metab. Rev. **43**:292–299.
6. **Arakane F, et al.** 1996. Steroidogenic acute regulatory protein (StAR) retains activity in the absence of its mitochondrial import sequence: implications for the mechanism of StAR action. Proc. Natl. Acad. Sci. U. S. A. **93**:13731–13736.
7. **Averette KM, et al.** 2009. Anthrax lethal toxin induced lysosomal membrane permeabilization and cytosolic cathepsin release is Nlrp1b/Nalp1b-dependent. PLoS One **4**:e7913. doi:10.1371/journal.pone.0007913.
8. **Bhatnagar R, Singh Y, Leppla SH, Friedlander AM.** 1989. Calcium is required for the expression of anthrax lethal toxin activity in the macrophagelike cell line J774A. 1. Infect. Immun. **57**:2107–2114.
9. **Biswas KK, et al.** 2003. Membrane cholesterol but not putative receptors mediates anandamide-induced hepatocyte apoptosis. Hepatology **38**: 1167–1177.
10. **Boveris A, Chance B.** 1973. The mitochondrial generation of hydrogen peroxide. General properties and effect of hyperbaric oxygen. Biochem. J. **134**:707–716.
11. **Boyden ED, Dietrich WF.** 2006. Nalp1b controls mouse macrophage susceptibility to anthrax lethal toxin. Nat. Genet. **38**:240–244.
12. **Broz P, von Moltke J, Jones JW, Vance RE, Monack DM.** 2010. Differential requirement for caspase-1 autoproteolysis in pathogen-induced cell death and cytokine processing. Cell Host Microbe **8**:471–483.
13. **Chandra H, et al.** 2005. Proteome analysis of mouse macrophages treated with anthrax lethal toxin. Biochim. Biophys. Acta **1747**:151–159.
14. **Charman M, Kennedy BE, Osborne N, Karten B.** 2010. MLN64 mediates egress of cholesterol from endosomes to mitochondria in the absence of functional Niemann-Pick type C1 protein. J. Lipid Res. **51**:1023–1034.
15. **Chen Q, Vazquez EJ, Moghaddas S, Hoppel CL, Lesnefsky EJ.** 2003. Production of reactive oxygen species by mitochondria: central role of complex III. J. Biol. Chem. **278**:36027–36031.
16. **Cheng JZ, et al.** 2001. Transfection of mGSTA4 in HL-60 cells protects against 4-hydroxynonenal-induced apoptosis by inhibiting JNK-mediated signaling. Arch. Biochem. Biophys. **392**:197–207.
17. **Choi K, Kim J, Kim GW, Choi C.** 2009. Oxidative stress-induced necrotic cell death via mitochondria-dependent burst of reactive oxygen species. Curr. Neurovasc. Res. **6**:213–222.
18. **Costes SV, et al.** 2004. Automatic and quantitative measurement of protein-protein colocalization in live cells. Biophys. J. **86**:3993–4003.
19. **Das ND, Jung KH, Chai YG.** 2010. The role of NF-kappaB and H3K27me3 demethylase, Jmjd3, on the anthrax lethal toxin tolerance of RAW 264.7 cells. PLoS One **5**:e9913. doi:10.1371/journal.pone.0009913.
20. **Dostert C, et al.** 2008. Innate immune activation through Nalp3 inflammasome sensing of asbestos and silica. Science **320**:674–677.
21. **Fernandez-Checa JC, Kaplowitz N.** 2005. Hepatic mitochondrial glutathione: transport and role in disease and toxicity. Toxicol. Appl. Pharmacol. **204**:263–273.
22. **Fernandez A, Llacuna L, Fernandez-Checa JC, Colell A.** 2009. Mitochondrial cholesterol loading exacerbates amyloid beta peptide-induced inflammation and neurotoxicity. J. Neurosci. **29**:6394–6405.
23. **Franchi L, Munoz-Planillo R, Nunez G.** 2012. Sensing and reacting to microbes through the inflammasomes. Nat. Immunol. **13**:325–332.
24. **Garcia-Ruiz C, Fernandez-Checa JC.** 2006. Mitochondrial glutathione: hepatocellular survival-death switch. J. Gastroenterol. Hepatol **21**(Suppl 3):S3–S6.
25. **Gross O, et al.** 2009. Syk kinase signalling couples to the Nlrp3 inflammasome for anti-fungal host defence. Nature **459**:433–436.
26. **Gross O, Thomas CJ, Guarda G, Tschopp J.** 2011. The inflammasome: an integrated view. Immunol. Rev. **243**:136–151.
27. **Ha SD, et al.** 2010. Cathepsin B-mediated autophagy flux facilitates the anthrax toxin receptor 2-mediated delivery of anthrax lethal factor into the cytoplasm. J. Biol. Chem. **285**:2120–2129.
28. **Ha SD, et al.** 2007. Mitochondrial proteins Bnip3 and Bnip3L are involved in anthrax lethal toxin-induced macrophage cell death. J. Biol. Chem. **282**:26275–26283.
29. **Ha SD, Park S, Hattlmann CJ, Barr SD, Kim SO.** 2012. Inhibition or deficiency of cathepsin B leads defects in HIV-1 Gag pseudoparticle release in macrophages and HEK293T cells. Antiviral Res. **93**:175–184.
30. **Hanna PC, Kruskal BA, Ezekowitz RA, Bloom BR, Collier RJ.** 1994. Role of macrophage oxidative burst in the action of anthrax lethal toxin. Mol. Med. **1**:7–18.
31. **Kilsdonk EP, et al.** 1995. Cellular cholesterol efflux mediated by cyclodextrins. J. Biol. Chem. **270**:17250–17256.
32. **Kim SO, et al.** 2003. Sensitizing anthrax lethal toxin-resistant macrophages to lethal toxin-induced killing by tumor necrosis factor-alpha. J. Biol. Chem. **278**:7413–7421.
33. **Kirkland RA, Franklin JL.** 2007. Bax affects production of reactive oxygen by the mitochondria of non-apoptotic neurons. Exp. Neurol. **204**:458–461.
34. **Korshunov SS, Skulachev VP, Starkov AA.** 1997. High protonic potential actuates a mechanism of production of reactive oxygen species in mitochondria. FEBS Lett. **416**:15–18.
35. **Lamkanfi M, et al.** 2008. Targeted peptidecentric proteomics reveals caspase-7 as a substrate of the caspase-1 inflammasomes. Mol. Cell. Proteomics **7**:2350–2363.
36. **Lavigne P, Najmanivich R, Lehoux JG.** 2010. Mammalian StAR-related lipid transfer (START) domains with specificity for cholesterol: structural conservation and mechanism of reversible binding. Subcell. Biochem. **51**: 425–437.
37. **Lepe-Zuniga JL, Klostergaard J.** 1990. Tolerance to endotoxin in vitro: independent regulation of interleukin-1, tumor necrosis factor and interferon alpha production during in vitro differentiation of human monocytes. Lymphokine Res. **9**:309–319.
38. **Li N, et al.** 2003. Mitochondrial complex I inhibitor rotenone induces apoptosis through enhancing mitochondrial reactive oxygen species production. J. Biol. Chem. **278**:8516–8525.
39. **Loving CL, et al.** 2009. Role of anthrax toxins in dissemination, disease progression, and induction of protective adaptive immunity in the mouse aerosol challenge model. Infect. Immun. **77**:255–265.
40. **Machida K, Tanaka T.** 1999. Farnesol-induced generation of reactive oxygen species dependent on mitochondrial transmembrane potential hyperpolarization mediated by F_0F_1-ATPase in yeast. FEBS Lett. **462**:108–112.
41. **Mari M, et al.** 2006. Mitochondrial free cholesterol loading sensitizes to TNF- and Fas-mediated steatohepatitis. Cell Metab. **4**:185–198.
42. **Martinon F.** 2010. Signaling by ROS drives inflammasome activation. Eur. J. Immunol. **40**:616–619.
43. **Moayeri M, et al.** 2010. Inflammasome sensor Nlrp1b-dependent resistance to anthrax is mediated by caspase-1, IL-1 signaling and neutrophil recruitment. PLoS Pathog. **6**:e1001222. doi:10.1371/journal.ppat.1001222.
44. **Orrenius S, Gogvadze V, Zhivotovsky B.** 2007. Mitochondrial oxidative stress: implications for cell death. Annu. Rev. Pharmacol. Toxicol. **47**:143–183.
45. **Raymond B, et al.** 2009. Anthrax lethal toxin impairs IL-8 expression in epithelial cells through inhibition of histone H3 modification. PLoS Pathog. **5**:e1000359. doi:10.1371/journal.ppat.1000359.
46. **Raza H.** 2011. Dual localization of glutathione S-transferase in the cytosol and mitochondria: implications in oxidative stress, toxicity and disease. FEBS J. **278**:4243–4251.
47. **Rigotti A, Cohen DE, Zanlungo S.** 2010. STARTing to understand MLN64 function in cholesterol transport. J. Lipid Res. **51**:2015–2017.
48. **Rone MB, Fan J, Papadopoulos V.** 2009. Cholesterol transport in steroid biosynthesis: role of protein-protein interactions and implications in disease states. Biochim. Biophys. Acta **1791**:646–658.
49. **Rosenbaum AI, Zhang G, Warren JD, Maxfield FR.** 2010. Endocytosis of beta-cyclodextrins is responsible for cholesterol reduction in Niemann-Pick type C mutant cells. Proc. Natl. Acad. Sci. U. S. A. **107**:5477–5482.

50. **Salles II, Tucker AE, Voth DE, Ballard JD.** 2003. Toxin-induced resistance in Bacillus anthracis lethal toxin-treated macrophages. Proc. Natl. Acad. Sci. U. S. A. **100**:12426–12431.
51. **Sapra R, et al.** 2006. Proteomic analyses of murine macrophages treated with Bacillus anthracis lethal toxin. Microb. Pathog. **41**:157–167.
52. **Scaduto RC, Jr., Grotyohann LW.** 1999. Measurement of mitochondrial membrane potential using fluorescent rhodamine derivatives. Biophys. J. **76**:469–477.
53. **Shao W, Yeretssian G, Doiron K, Hussain SN, Saleh M.** 2007. The caspase-1 digestome identifies the glycolysis pathway as a target during infection and septic shock. J. Biol. Chem. **282**:36321–36329.
54. **Shin S, et al.** 2000. Intracellular calcium antagonist protects cultured peritoneal macrophages against anthrax lethal toxin-induced cytotoxicity. Cell Biol. Toxicol. **16**:137–144.
55. **Shin S, Kim YB, Hur GH.** 1999. Involvement of phospholipase A2 activation in anthrax lethal toxin-induced cytotoxicity. Cell Biol. Toxicol. **15**:19–29.
56. **Soccio RE, Breslow JL.** 2003. StAR-related lipid transfer (START) proteins: mediators of intracellular lipid metabolism. J. Biol. Chem. **278**: 22183–22186.
57. **Squires RC, Muehlbauer SM, Brojatsch J.** 2007. Proteasomes control caspase-1 activation in anthrax lethal toxin-mediated cell killing. J. Biol. Chem. **282**:34260–34267.
58. **Strowig T, Henao-Mejia J, Elinav E, Flavell R.** 2012. Inflammasomes in health and disease. Nature **481**:278–286.
59. **Terra JK, et al.** 2010. Cutting edge: resistance to Bacillus anthracis infection mediated by a lethal toxin sensitive allele of Nalp1b/Nlrp1b. J. Immunol. **184**:17–20.
60. **Tichauer JE, et al.** 2007. Overexpression of the cholesterol-binding protein MLN64 induces liver damage in the mouse. World J. Gastroenterol. **13**:3071–3079.
61. **Ting JP, Willingham SB, Bergstralh DT.** 2008. NLRs at the intersection of cell death and immunity. Nat. Rev. Immunol. **8**:372–379.
62. **Warren MK, Vogel SN.** 1985. Bone marrow-derived macrophages: development and regulation of differentiation markers by colony-stimulating factor and interferons. J. Immunol. **134**:982–989.
63. **Watari H, et al.** 1997. MLN64 contains a domain with homology to the steroidogenic acute regulatory protein (StAR) that stimulates steroidogenesis. Proc. Natl. Acad. Sci. U. S. A. **94**:8462–8467.
64. **Wickliffe KE, Leppla SH, Moayeri M.** 2008. Anthrax lethal toxin-induced inflammasome formation and caspase-1 activation are late events dependent on ion fluxes and the proteasome. Cell Microbiol. **10**:332–343.
65. **Zhang M, et al.** 2002. MLN64 mediates mobilization of lysosomal cholesterol to steroidogenic mitochondria. J. Biol. Chem. **277**:33300–33310.
66. **Zhou R, Yazdi AS, Menu P, Tschopp J.** 2011. A role for mitochondria in NLRP3 inflammasome activation. Nature **469**:221–225.
67. **Zimniak L, Awasthi S, Srivastava SK, Zimniak P.** 1997. Increased resistance to oxidative stress in transfected cultured cells overexpressing glutathione S-transferase mGSTA4-4. Toxicol. Appl. Pharmacol. **143**:221–229.
68. **Zuckerman SH, Evans GF, Butler LD.** 1991. Endotoxin tolerance: independent regulation of interleukin-1 and tumor necrosis factor expression. Infect. Immun. **59**:2774–2780.